Cell Reports

Article

Polyphosphate degradation by Nudt3-Zn^{2+} mediates oxidative stress response

Graphical abstract

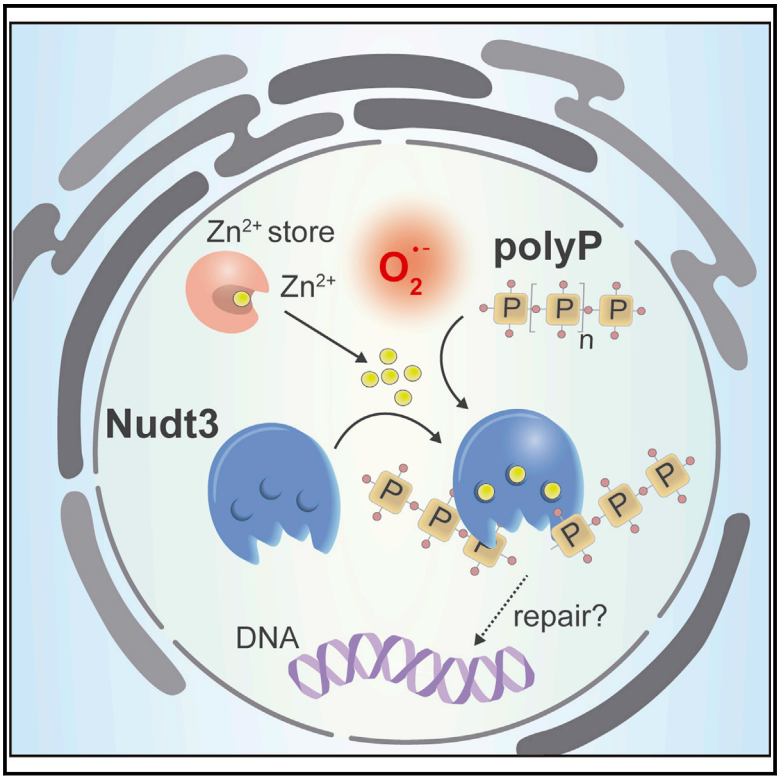

Authors

Bàrbara Samper-Martín, Ana Sarrias, Blanca Lázaro, ..., Adolfo Saiardi, Javier Jiménez, Samuel Bru

Correspondence

jjimenez@uic.es (J.J.), sbru@uic.es (S.B.)

In brief

Samper-Martín et al. show that polyphosphate, a chain of orthophosphates, plays an essential role in oxidative stress response in human cells. In addition, they identify the human Nudt3 as a polyphosphate hydrolase, opening the door to modifying polyphosphate content, a tool to advance understanding of mammalian polyphosphate metabolism.

Highlights

- An unbiased screen reveals Nudt3 as a metazoan polyphosphate hydrolase
- Nudt3 is activated *in vitro* and *in vivo* by Zn^{2+}
- Oxidative stress mobilizes Zn^{2+}, which activates Nudt3 to degrade polyphosphate
- Polyphosphate degradation is essential for cell survival upon oxidative stress

Samper-Martín et al., 2021, Cell Reports *37*, 110004
November 16, 2021
https://doi.org/10.1016/j.celrep.2021.110004

CellPress

Cell Reports

CellPress
OPEN ACCESS

Article

Polyphosphate degradation by Nudt3-Zn^{2+} mediates oxidative stress response

Bàrbara Samper-Martín,[1] Ana Sarrias,[1] Blanca Lázaro,[1] Marta Pérez-Montero,[1] Rosalía Rodríguez-Rodríguez,[1] Mariana P.C. Ribeiro,[1] Aitor Bañón,[2] Don Wolfgeher,[3] Henning J. Jessen,[4,5] Berta Alsina,[2] Josep Clotet,[1] Stephen J. Kron,[3] Adolfo Saiardi,[6] Javier Jiménez,[1,8,*] and Samuel Bru[1,7,*]

[1]Faculty of Medicine and Health Sciences, Universitat Internacional de Catalunya, 08195 Sant Cugat del Vallès, Barcelona, Spain
[2]Department of Experimental and Health Sciences, Universitat Pompeu Fabra-Parc de Recerca Biomèdica, 08003 Barcelona, Spain
[3]Department of Molecular Genetics and Cell Biology, University of Chicago, Chicago, IL 60637, USA
[4]Institute of Organic Chemistry, University of Freiburg, 79104 Freiburg, Germany
[5]CIBSS – Centre for Integrative Biological Signalling Studies, University of Freiburg, 79104 Freiburg, Germany
[6]Medical Research Council Laboratory for Molecular Cell Biology, University College London, London WC1E6BT, UK
[7]Institut de Neurociències, Universitat Autònoma de Barcelona, 08193 Bellaterra, Cerdanyola del Vallès, Spain
[8]Lead contact
*Correspondence: jjimenez@uic.es (J.J.), sbru@uic.es (S.B.)
https://doi.org/10.1016/j.celrep.2021.110004

SUMMARY

Polyphosphate (polyP) is a polymer of hundreds of phosphate residues present in all organisms. In mammals, polyP is involved in crucial physiological processes, including coagulation, inflammation, and stress response. However, after decades of research, the metabolic enzymes are still unknown. Here, we purify and identify Nudt3, a NUDIX family member, as the enzyme responsible for polyP phosphatase activity in mammalian cells. We show that Nudt3 shifts its substrate specificity depending on the cation; specifically, Nudt3 is active on polyP when Zn^{2+} is present. Nudt3 has *in vivo* polyP phosphatase activity in human cells, and importantly, we show that cells with altered polyP levels by modifying Nudt3 protein amount present reduced viability upon oxidative stress and increased DNA damage, suggesting that polyP and Nudt3 play a role in oxidative stress protection. Finally, we show that Nudt3 is involved in the early stages of embryo development in zebrafish.

INTRODUCTION

Inorganic polyphosphate (polyP) is a molecule of heterogeneous size consisting of a few to several thousand ortho-phosphates (Pi) linked by phospho-anhydride bonds (Kornberg, 1999). PolyP was first described more than a century ago (Babes, 1895) and has been observed in microorganisms and metazoans (Brown and Kornberg, 2004; Kulaev and Vagabov, 1983; Kumble and Kornberg, 1995; Smith et al., 2006). In unicellular organisms, polyP displays several and diverse functions, including energy and/or phosphate reservoir, cation chelation, stress protection, cell-cycle progression, DNA repair, protein folding, and signaling (Albi and Serrano, 2016; Desfougerès et al., 2020; Jiménez et al., 2017). In metazoans, extracellular polyP has been reported to be involved in diverse functions, including inflammation (Hassanian et al., 2017), blood clotting (Nickel et al., 2015; Travers et al., 2015), and protein aggregation (Cremers et al., 2016). In addition, intracellular polyP has been implicated in cell differentiation (Morimoto et al., 2010), transcriptional regulation (Jimenez-Nuñez et al., 2012), cell signaling (Azevedo et al., 2015), and DNA repair (Bru et al., 2017). Nonetheless and importantly, dissecting the mechanisms of polyP in cell regulation has remained hampered by a poor understanding of the pathways and enzymes responsible for synthesis and degradation (Bondy-Chorney et al., 2020; Desfougerès et al., 2020) despite concerted efforts.

Following their observations of polyP in the brain, Kumble and Kornberg (1996) also observed high levels of endo-polyP phosphatase (endo-polyPase; degrades polyP cleaving internal bounds) activity in rat brain homogenate that cleaved the long chains into smaller fragments. Most efforts at the discovery of metazoan polyPases have been based on exploiting homology to polyPases from prokaryotes and simple eukaryotes leading to h-prune and DIPPs (diphosphoinositol-pyrophosphate-polyphosphatases). The human protein phosphatase h-prune shares remarkable homology to the yeast Ppx1 exo-polyPase (degrades polyP from the molecule ends), but it has substrate-specificity constrictions that are difficult to reconcile with the polyPase activity; in fact, it is inhibited in the presence of medium to long polyP (Tammenkoski et al., 2008). DIPPs are a subfamily of NUDIX proteins (see below) that, despite sharing a remarkable homology with the yeast Ddp1 endo-polyPase, shows low *in vitro* activity and is restricted to pH 9.5 values far from physiologic (Lonetti et al., 2011). In a similar scenario is *T. brucei* homolog (Cordeiro et al., 2019).

MutT/NUDIX (cleaves nucleoside diphosphate linked to some other moiety X) is an evolutionarily conserved family of 22

Table 1. Purification parameters

Step	Protein (mg)	Specific activity (μmol/min·mg)	Total activity	Purification (-fold)	Yield (%)
Homogenate	226	27	6,116	1	100
Supernatant	120	28	3,382	1.04	55
Heparin	4.8	156	742	5.7	12.1
Superdex	0.1	1,984	223	73.3	3.7

Rat brain tissues were homogenized and cells lysed. Protein total amount and specific endo-polyPase activity were measured as described in STAR Methods. Enzymatic parameters for the purification steps are provided.

hydrolases, including divalent cation-regulated enzymes that hydrolyze diverse dinucleotides and inositol pyrophosphates (PP-InsPs), among a wide range of substrates. DIPPs subfamily, including Nudt3, Nudt4, Nudt10, and Nudt11, have previously been linked to the degradation of InsPs and di-adenosine-polyPs (Ap_nA) (Carreras-Puigvert et al., 2017). Remarkably DIPPs, and particularly Nudt3, present a strong substrate specificity according to the cation, and hydrolysis of PP-InsPs requires magnesium (Mg^{2+}) (Kilari et al., 2013; Safrany and Shears, 1998) versus manganese (Mn^{2+}) for Ap_nA (Safrany et al., 1999). Nudt3 has also been ascribed an important *in vivo* function in decapping mRNAs, also dependent on Mn^{2+} (Grudzien-Nogalska et al., 2016; Sahu et al., 2020). A similar scenario occurs in polyPases activity regulation; specifically, zinc (Zn^{2+}) and cobalt (Co^{2+}) are used by yeast endo-polyPase Ppn2 (Gerasimaitė and Mayer, 2017). In mammalian cells, most Zn^{2+} remains sequestered by metallothioneins (MTs) (Stankovic et al., 2007), small cysteine-rich metal-binding proteins that serve an important role in oxidative stress response. Free Zn^{2+} is normally kept low in cells, in large part via buffering by MTs. However, increased reactive oxygen species leads to oxidation of MTs thiols, releasing bound Zn^{2+} from coordination (Maret, 2011). Total Zn^{2+} abundance and, likely, activity is higher in the brain (Frederickson et al., 2005), where it has been implicated in signaling, differentiation, and synaptic function (Beyersmann and Haase, 2001).

Here, we reexamined the long-ago described endo-polyPase activity in the mammalian brain (Kumble and Kornberg, 1996) to discover a physiological endo-polyPase. Surprisingly, this work pointed back to Nudt3, but activated by Zn^{2+}, a cation of outstanding importance in the brain, maintained at low levels but released from MTs upon oxidative stress. Here, we establish this NUDIX protein as a Zn^{2+}-dependent polyPase that plays a critical role *in vivo* in limiting DNA damage and maintaining cell survival upon oxidative stress.

RESULTS

Mammalian polyP phosphatase purification

Consistent with prior studies (Lorenz et al., 1997), the adult rat brain is the organ that contains the highest levels of polyP, although with significant differences among major brain structures (Figure S1A). Toward identifying the polyP-degrading activity identified by Kumble and Kornberg (1996), we enriched an endo-polyPase activity from rat brain homogenates (Table 1). In brief, the resulting supernatant, retaining about half the activity and similar specific activity to homogenate, was applied to a heparin affinity column. Several yeast polyPases can be bound by heparin (Andreeva et al., 2015; Lichko et al., 1998), reflecting the negative charge of the polyP. Indeed, TAP-tagged Ppx1 and Ppn1 were readily adsorbed onto the heparin column from yeast cell extracts and eluted with high salt (Figure S1B). Similarly, brain extract fractions were eluted with a NaCl gradient and assayed for endo-polyPase activity by detecting cleavage of high-molecular-weight polyP, using PAGE-urea gels. By performing assays with Mg^{2+}, Ca^{2+}, Co^{2+}, Mn^{2+}, and Zn^{2+}, we found a prominent endo-polyPase activity stimulated by Zn^{2+} that eluted at 0.5 M NaCl that also displayed residual activity by Mg^{2+} and Mn^{2+} (Figures 1A and S1C–S1E). When peak fractions were separated by size exclusion chromatography, the Zn^{2+}-dependent activity was eluted at low molecular weight.

The apparent purification of 70-fold was insufficient to point to a single protein band using PAGE. Thus, we developed an "in-gel" polyP degradation assay, which we dubbed the polyP-zymogram. In brief, protein fractions were separated on native polyacrylamide gels in Tris-borate-EDTA (TBE) buffer containing embedded long-chain polyP. After incubating the gels in polyPase reaction buffer, in-gel cleavage was assessed by loss of DAPI staining. As a proof of concept, a sample of purified yeast endo-polyPase Ddp1 produced a completely cleared band (Figure 1B, left). Similarly, the peak fraction of brain endo-polyPase activity eluted from size exclusion chromatography led to a single band that was cut from the gel and analyzed by tandem mass spectrometry (Figure 1B, right). Among the 10 most confident protein identifications was the NUDIX family protein Nudt3, previously suggested as a candidate endo-polyPase (Lonetti et al., 2011). Nudt3 is broadly expressed in human tissues but at particularly high levels in multiple brain structures (Figure S1F).

Nudt3 is a Zn^{2+}-dependent human polyPase

To confirm human Nudt3 as polyPase, we assayed purified *E. coli*-expressed recombinant human GST-Nudt3 fusion protein for cleavage of polyP, revealing a requirement for Zn^{2+} (Figure 1C). Similarly, Nudt3 protein purified from HEK293T human embryonic kidney cells displayed a Zn^{2+}-dependent polyPase with a similar specific activity (Figure 1D) suggesting no post-translational modifications. To further characterize the polyPase activity, we examined its pH dependence (Figure 1E). Taking into account that polyP is unstable at alkaline pH in the presence of divalent cations (Harold, 1966), GST-Nudt3 displayed strong polyPase activity at pH 6.8 and 7.4. The enzyme was fully inhibited by broad phosphatase inhibitors NaF, NaPPi, or β-glycerol phosphate, as well as by the polyPase inhibitor heparin (Figure 1F). Site-directed mutagenesis of the Nudt3 catalytic residue E70 to A (Safrany et al., 1999) and expression of GST-$Nudt3^{E70A}$

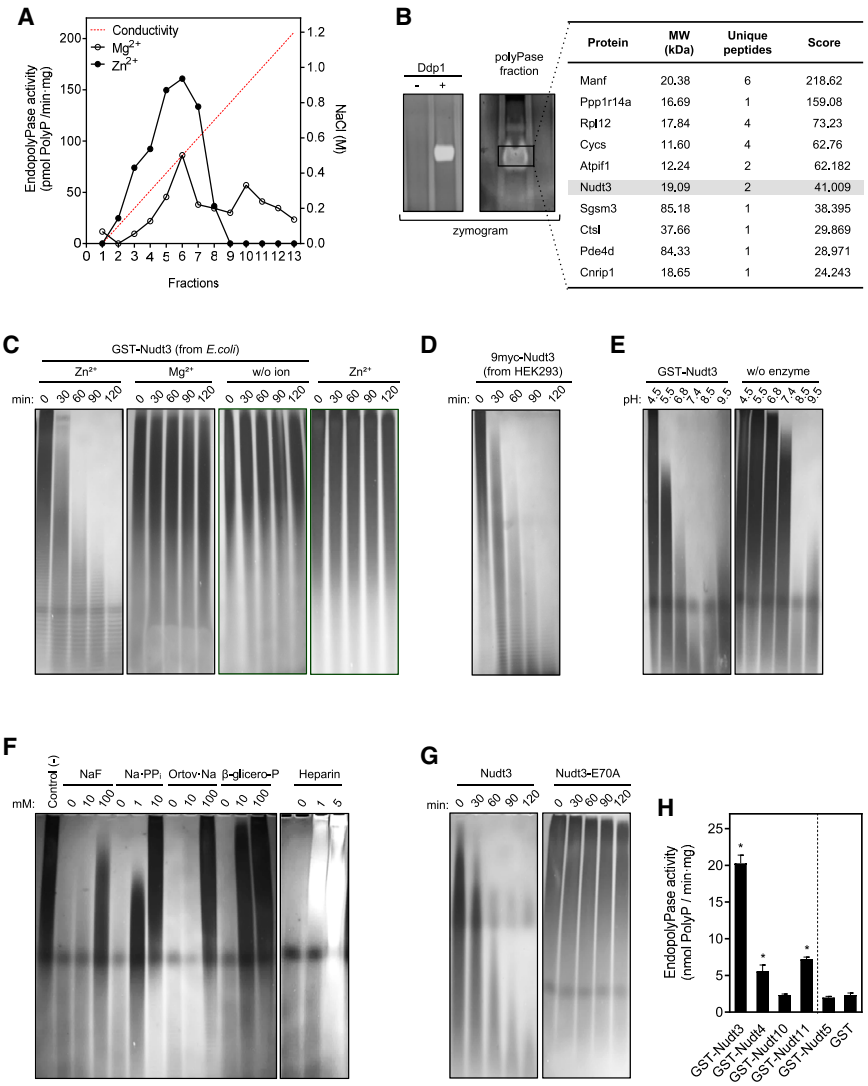

Figure 1. Nudt3 is a Zn^{2+}-dependent endo-polyPase

(A) Heparin affinity fractionation step. After tissue homogenization, cell lysis, and centrifugation, the supernatant was loaded into a heparin-based affinity chromatography column. Proteins were eluted by applying a NaCl-based ionic strength gradient (dashed line). Endo-polyPase activity was assayed using the indicated divalent cations (see STAR Methods section).

(B) PolyP-zymogram and mass spectrometry identification. The left panel shows a proof of concept for the polyP-zymogram: recombinant yeast Ddp1 was separated in a non-denaturing acrylamide gel containing polyP. polyPase activity was permitted by incubating the gel in the appropriate conditions. The gel was stained with DAPI. In the right panel, containing activity aliquot from the size exclusion column was analyzed in the polyP-zymogram as above. The area where the polyPase activity appeared was excised, and proteins were identified by tandem mass spectrometry analysis. A list of the proteins showing the higher score is provided.

(C and D) Human Nudt3 obtained from *E. coli* (C) and the HEK293T cell line (D) have Zn^{2+}-dependent endo-polyPase activity. Nudt3 was incubated with 5 μg of $polyP_{100}$ for the indicated times in the presence of 5 mM of the noted cations, electrophoretically separated in PAGE-urea gels, and polyP was visualized using DAPI staining.

(E) Nudt3 is active at physiological pH. Nudt3 was incubated at different pH values with 5 μg of $polyP_{100}$; polyP was separated in PAGE-urea gels and stained with DAPI.

(F) Nudt3 endo-polyPase activity is inhibited by phosphatase inhibitors. As in (C), using 5 mM Zn^{2+} as a cation and the concentration of the noted inhibitors. Incubation time was 1 h.

(G) $Nudt3^{E70A}$ does not present endo-polyPase activity. As in (C) using 5 mM Zn^{2+}.

(H) Endo-polyPase activity quantification of the different members of the human DIPP family purified from *E. coli*. As in (C) using 5 mM Zn^{2+}. Incubation time was 1 h. Mean ± SEM of three independent experiments. ***$p < 0.001$; **$p < 0.01$; *$p < 0.05$.

See also Figures S1 and S2.

yielded no activity (Figure 1G). By comparison, GST fusions of other DIPP subfamily NUDIX proteins, Nudt4, Nudt10, and Nudt11, displayed only a fraction of the Zn^{2+}-dependent activity of Nudt3 (Figures 1H and S2A). The distantly related NUDIX protein Nudt5 did not display endo-polyPase activity (Figures 1H and S2A).

Nudt3 substrate specificity depends on the divalent cation

Based on the several cations usage by Nudt3, we wondered whether Nudt3 could use other divalent cations to degrade polyP. We examined endo-polyPase activity by PAGE-urea gel and exo-polyPase by the malachite green method, comparing with the yeast proteins Ddp1 and Ppx1, respectively, in the presence of Zn^{2+}, Co^{2+}, Mn^{2+}, and Mg^{2+} or without divalent cation (Figures 2A and 2B). GST-Nudt3 displayed robust endo-polyPase activity with Zn^{2+} and Mn^{2+}(Figure 2A), but little or no exo-polyPase with any cation (Figure 2B). PAGE-urea gels pattern, Ddp1 homology, and exo-polyPase assay strongly suggest an endo-polyPase activity for Nudt3, although we cannot totally exclude some exo-polyPase activity.

The 22 human NUDIX enzymes can hydrolyze a structurally diverse range of substrates but display distinct patterns of specificity (Caffrey et al., 2000; Carreras-Puigvert et al., 2017; Kilari et al., 2013). Our results raised the question of whether cations might determine substrate specificity for Nudt3. Thus, we compared hydrolysis of polyP and two well-described Nudt3 substrates, 5-diphosphoinositol pentakisphosphate (5-InsP7) (Safrany et al., 1998) and P1, P5-Di(adenosine-5′) pentaphosphate (Ap5A) (Safrany et al., 1999) in the presence of Mg^{2+},

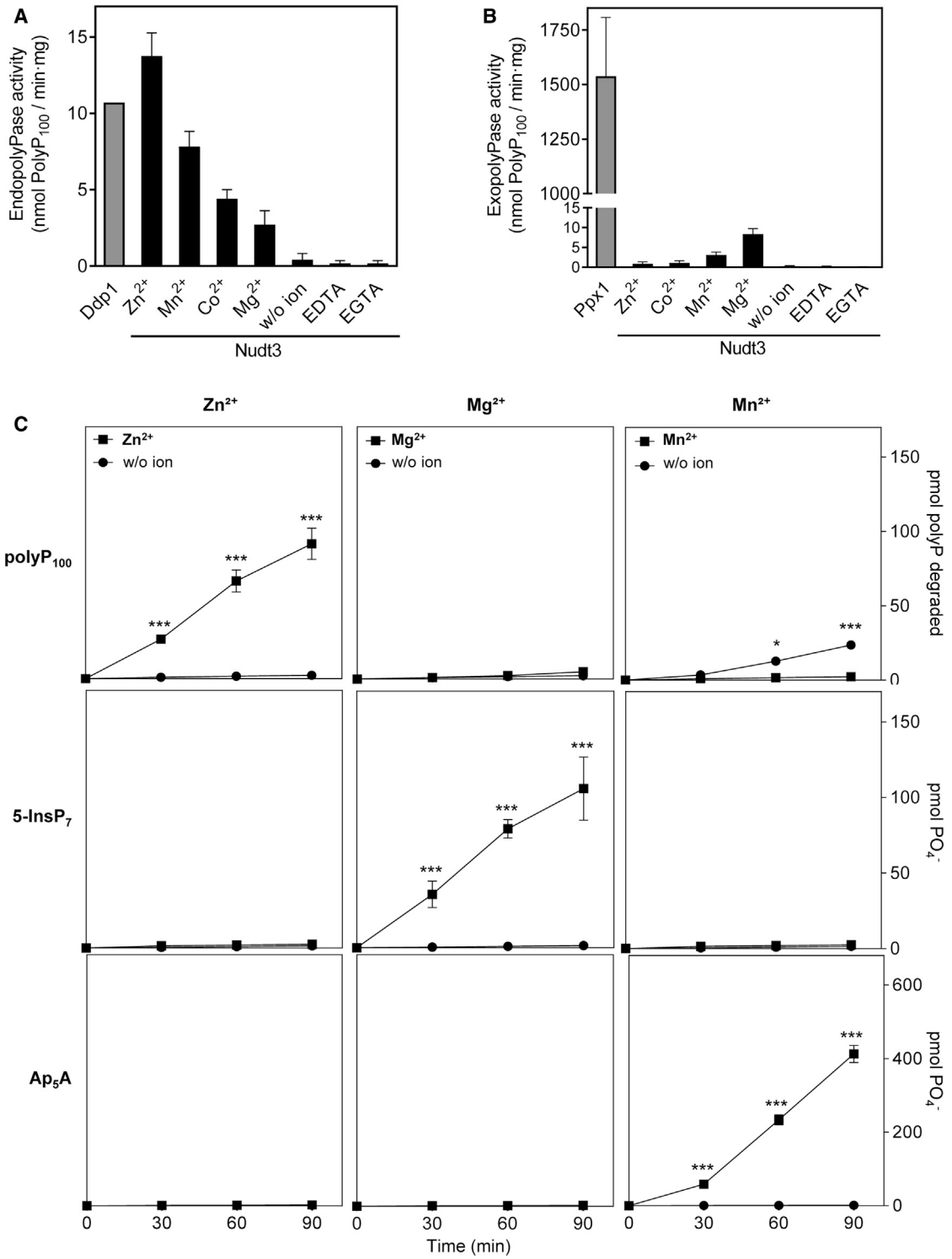

Figure 2. Nudt3 substrate specificity is ion dependent

(A) Divalent ion dependence of Nudt3 endo-polyPase activity. Quantification of DAPI-stained PAGE-urea gels as in Figure 1. Nudt3 (100 ng) and polyP$_{100}$ were incubated for 1 h in the presence of the mentioned ions (5 mM each), EDTA, or EGTA (10 mM). 100 ng of yeast recombinant endo-polyPase Ddp1 (Nudt3 homolog) is used as control. Mean ± SEM of three independent experiments.

(legend continued on next page)

Zn^{2+}, or Mn^{2+} (Figure 2C). Although polyP cleavage was dependent on Zn^{2+}, we observed hydrolysis of 5-InsP7 by Nudt3 only in the presence of Mg^{2+}. In turn, Nudt3 was able to cleave Ap5A, but only in the presence of Mn^{2+}.

Nudt3 is a polyPase *in vivo*

First, we confirmed the presence of Nudt3 in HEK293T cells by immunofluorescence using specific antibodies and revealed ubiquitous localization, including nucleus that was reduced by siRNA knockdown (Figure S2B). To examine polyPase activity, we tracked endogenous polyP levels by detecting binding of Xpress-tagged *E. coli* exo-polyPase polyP binding domain (PPBD) to cellular polyP (Saito et al., 2005). Immunodetection of PPBD revealed nuclear foci in HEK293T cells that were lost after treatment of the fixed and permeabilized cells with purified yeast exo-polyPase Ppx1, establishing specificity for polyP (Figure 3A). Knockdown of endogenous Nudt3 by siRNAs resulted in increased PPBD signal, indicating accumulation of polyP (Figures 3B and S2C). Overexpression of Ppx1 or Nudt3 reduced PPBD binding, consistent with decreased polyP levels (Figures 3C and S2D). In turn, expression from a doxycycline-inducible promoter led to regulated increased Nudt3 protein and a corresponding decrease in polyP content (Figures 3D, 3E, and S2E). According to these genetic approaches, we conclude that Nudt3 represents an *in vivo* regulator of polyP amount.

Nudt3 *in vivo* polyPase activity is Zn^{2+} dependent

Although Nudt3 displays robust polyPase activity, its cation dependence raises the question of whether this may not be relevant in cells where Zn^{2+} is largely kept sequestered. Toward establishing the cation dependence of the endogenous Nudt3 activity, HEK293T cells were incubated for 48 h in media containing 0.1 mM Zn^{2+} obtaining markedly decreased polyP nuclear foci (Figure 4A). PolyP was restored by adding the non-specific divalent ion chelator Na-EDTA or the Zn^{2+} chelator sodium hydrosulfide (NaHS) without affecting cell viability (Figures 4A and S2F). Unlike Zn^{2+}, adding 0.1 mM Mg^{2+} did not reduce the polyP amount at 24 or 48 h (Figure 4B). Although HEK293 cells have been considered neuron-like cells (Stepanenko and Dmitrenko, 2015), we decided to confirm the Zn^{2+}-dependent polyP amount in another neuron cell line. Similar behavior was observed upon treating SH-SY5Y cells with 0.1 mM Zn^{2+} for 48 h (Figure 4C). Importantly, knockdown of Nudt3 suppressed the Zn^{2+}-dependent loss of polyP in HEK293T cells (Figures 4D and S2G). Neither Zn^{2+} nor Mg^{2+} impacted levels of 5-InsP7 (Figure 4E), arguing against an indirect effect on polyP cleavage mediated by substrate competition (Sahu et al., 2020). Taken together, these results implicate human Nudt3 as a Zn^{2+}-dependent endo-polyPase *in vivo*.

Nudt3 plays a role in cell survival upon oxidative stress

Although Zn^{2+} is normally sequestered by MTs, oxidative stress can induce Zn^{2+} release, leading to a transient increase in intracellular Zn^{2+} (Maret, 2000). In such context, Nudt3 polyPase activity might then be activated by the free Zn^{2+}, raising the question of whether polyP hydrolysis might be a component of the oxidative stress response (Figure 5A). As described previously (Aizenman et al., 2000), exposing HEK293T cells to hydrogen peroxide (H_2O_2) led to a rapid increase in free Zn^{2+}, as detected by the cell-permeable fluorogenic Zn^{2+} probe Zinpyr-1 both by fluorescence-activated cell sorting (FACS) (Figure 5B) and by microscopy inspection (Figure S3A), and a concomitant decrease in cellular polyP (Figure 5C), polyP decrease that is Nudt3 dependent as far as it cannot be observed when Nudt3 is depleted (Figure 5D). Importantly, polyP decrease and Nudt3 dependency are also obtained by exposing the cells to 15 μM menadione, an alternative oxidative stress-inducing agent (Figures S3B and S3C). Suggesting a critical role for Zn^{2+}/Nudt3 polyPase activity in oxidative stress response, siRNA knockdown of Nudt3 in both HEK293T and SH-SY5Y cells reduced cell survival after treatment with H_2O_2, as measured by MTT and colony-forming assays (Figures 5E and S3E). Interestingly, silencing or knocking down Nudt3 by specific CRISPR-Cas9 editing led to similar sensitivity to oxidative stress (Figure S3D). In turn, depleting polyP by overexpressing Nudt3 decreased HEK293T cell viability after exposure to H_2O_2 (Figures 5F and S3F). Note that overexpressing and depleting Nudt3 determine a similar effect in the cells: polyP reduction and inability to use it, respectively. Although polyP levels may affect cellular energy metabolism (Pavlov et al., 2010), we found no correlation between Nudt3 knockdown and cellular ATP levels after oxidative stress (Figure S4A).

Oxygen free radicals released by H_2O_2 target multiple cellular nucleophiles, including proteins, lipids, nucleic acids (including DNA double-strand breaks [DSBs]), and metabolites, leading to cellular damage. To assess a potential role for Nudt3 and its polyPase activity in DSB formation and repair, we examined the presence of the DSB marker γH2AX in cells after oxidative stress. In a time course, Nudt3 knockdown HEK293T cells displayed higher γH2AX levels than control cells at basal conditions, a difference that importantly increased after exposure to H_2O_2 (Figures 5G and S4B). In addition, we also detected the increase in γH2AX foci by immunofluorescence (Figure 5H). Finally, we obtained similar results silencing Nudt3 (Figure S4C). These experiments suggest that Nudt3 plays a role in DSB repair after oxidative stress in a time framework coherent with the Zn^{2+} release and polyP degradation.

Role of Nudt3 in early development

In zebrafish, Nudt3 is encoded by two genes, zNudt3a and zNudt3b. Recombinant zNudt3a displayed similar endo-polyPase activity to human Nudt3 (Figure S5A). Injection of a cocktail of eight guide RNAs complexed to Cas9 targeting the two genes was injected into one cell's embryos, yielding mosaics with incomplete disruption of the two genes (Figure S5B). At 8 days post-fertilization, massive morphological aberrations (Figure S5C)

(B) Exo-polyPase activity of Nudt3. The enzymatic reaction was as in (A). The activity was measured as free phosphate production using the malachite green method. Yeast recombinant exo-polyPase Ppx1 (1 ng) is used as a control. Mean ± SEM of three independent experiments.
(C) Enzymatic activity quantification of Nudt3 on the noted substrates (up to down: $polyP_{100}$, $5\text{-}InsP_7$, and Ap5A) in the presence of the indicated cations (5 mM). Mean ± SEM of three independent experiments. ***$p < 0.001$; **$p < 0.01$; *$p < 0.05$.

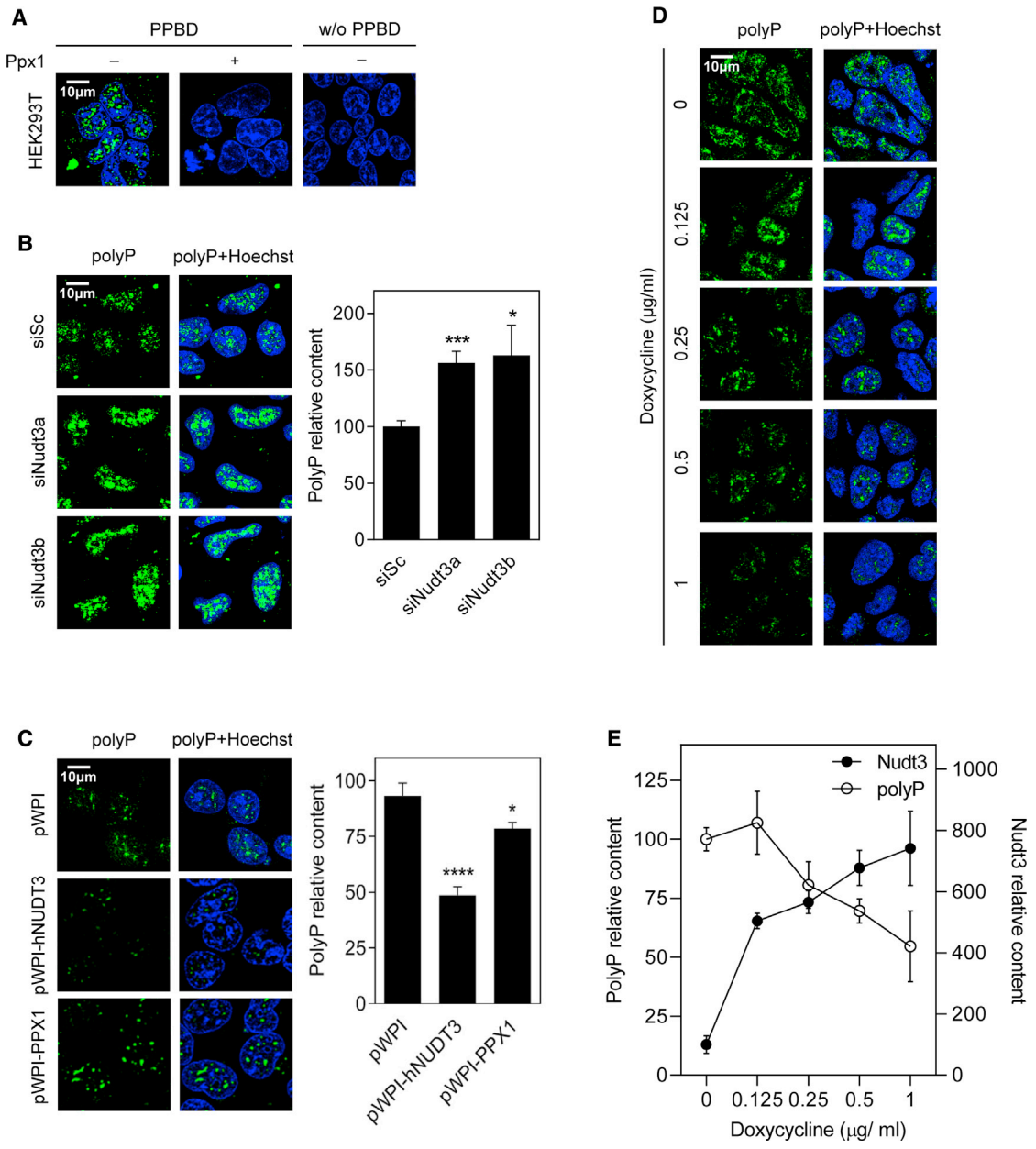

Figure 3. Nudt3 is a polyPase *in vivo*

(A) Validation of polyP signal detection. Immunofluorescence images of HEK293T human cells where polyP was detected using Xpress-PPBD (Xpress-tagged version of *E. coli* polyP binding domain protein), coupled with anti-Xpress antibody and anti-goat Alexa488 conjugated secondary antibody. Cells were treated (or not) with 1 µg of yeast exo-polyPase to deplete polyP and show specificity for polyP signal. Nuclei were stained using Hoechst. Negative control was without Xpress-PPBD.

(B) Nudt3 silencing increases nuclear polyP content. HEK293T cells were transfected with scrambled (Sc) RNA (10 nM) or with two different Nudt3-targeting siRNA (siNudt3a and siNudt3b) at 10 nM. After 48 h, polyP was detected as in (A). Representative images are in the left panel. The graph is for quantification (see STAR Methods) representing the mean ± SEM of at least eight different pictures from four independent experiments. A minimum of 500 cells per condition were analyzed.

(C) Constitutive overexpression of human Nudt3 decreases nuclear polyP content. HEK293T human cells were transfected with empty pWPI, pWPI-*hNUDT3*, or pWPI-sc*PPX1* (*S. cerevisiae* exo-polyPase). Polyphosphate was detected as in (A). Representative images are in the left panel. Quantification of 20 pictures from three independent experiments with a minimum of 1,300 cells per condition is in the right panel. Mean ± SEM is presented.

(D and E) Nudt3 depletes nuclear polyP in a dose-dependent manner. HEK293T human cells were transfected with empty pAdvanced and pRetroX or pAdvanced and pRetroX-hNudt3 permitting the expression of the human Nudt3 gene by adding different amounts of doxycycline. 48 h after transfection, the indicated amount of doxycycline was added, and after 72 h polyP was detected as in (A). (D) Representative images. (E) Quantification of at least five pictures of three independent experiments. A minimum of 200 cells per condition were analyzed. Mean ± SEM is provided.

The scale bars represent 10 µm. See also Figure S2. ***$p < 0.001$; **$p < 0.01$; *$p < 0.05$.

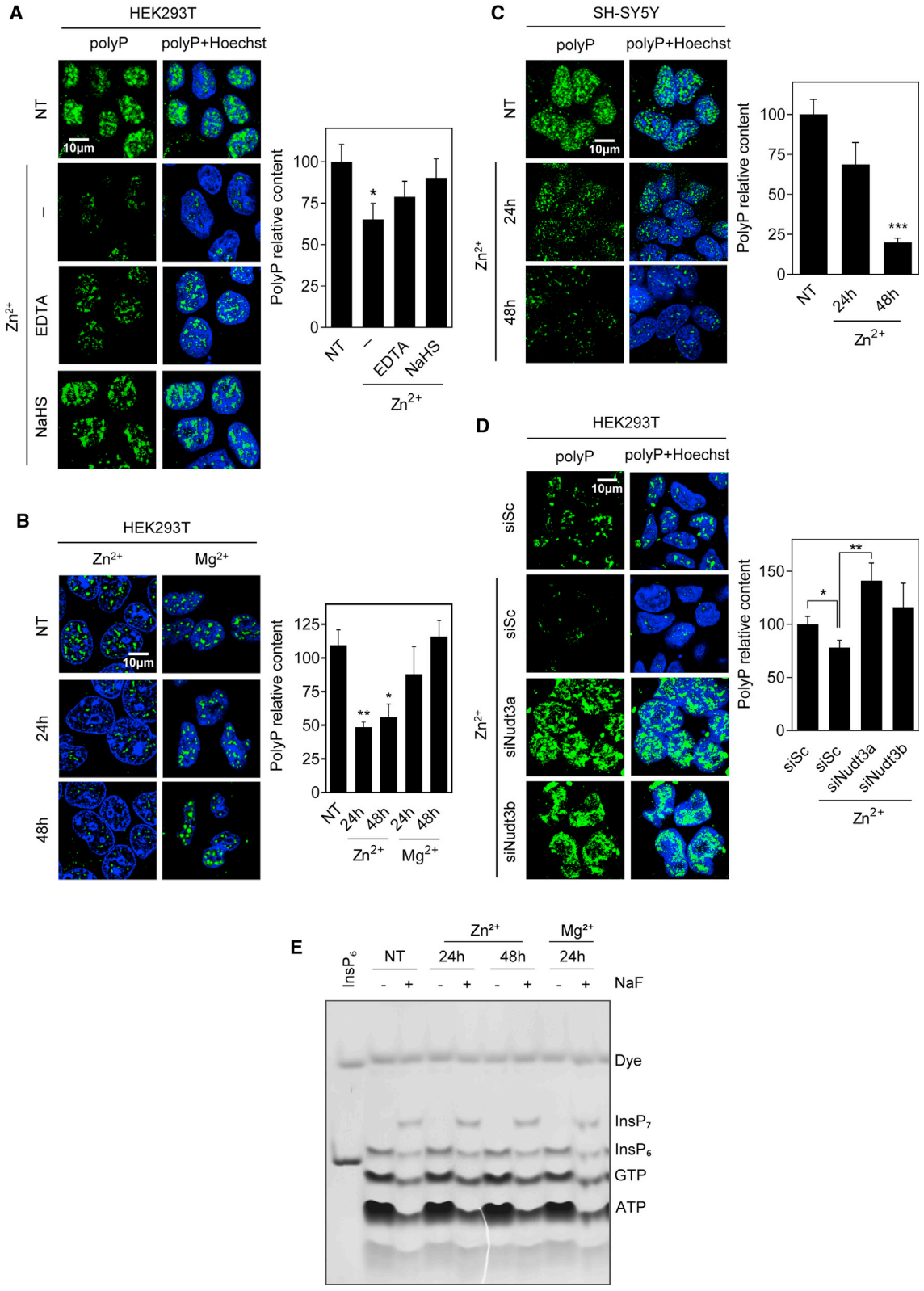

(legend on next page)

were observed in approximately half of the surviving animals. We decided thus to establish Nudt3 knockout lines for each gene; for this, we injected four guides targeting one gene in one-cell-stage embryos and crossed the surviving animals with wild-type (F1 generation). Heterozygous knockouts were backcrossed (F2 generation). Interestingly, none of the surviving F2 fish were homozygous knockouts for either gene (Figures S5D and S5E). The role of Nudt3 in brain development is supported by a peak of expression of human DIPP subfamily NUDIX proteins Nudt3, Nudt10, and Nudt11 before and following birth (Figure S1F), with Nudt3 being highly present in brain tissues (Figure S5F) where polyP and Zn^{2+} are especially abundant, a striking correlation that deserves further investigation.

DISCUSSION

PolyP study runs at two velocities: in simple genetic models, it moves fast, whereas it is lagging in metazoans. The main reason for the extra difficulty in studying polyP in mammalian cells and organisms lies in our ignorance of the enzymes responsible for their synthesis and degradation, making difficult the manipulation of polyP levels; consequently, its functional roles are poorly defined in metazoans. This impediment has been addressed by using well-known polyPases from other organisms, such as bacteria (Bondy-Chorney et al., 2020) and yeast (Bru et al., 2017; Wang et al., 2003). Here, we have identified the NUDIX family hydrolase Nudt3 as responsible for an abundant Zn^{2+} cation-dependent polyP cleaving activity. We find that Zn^{2+}-activated Nudt3 functions as an endogenous polyPase in human cells, with roles in maintaining cell viability in the face of oxidative stress. When cells are treated with H_2O_2, Zn^{2+} quick release from MTs activates Nudt3 to degrade the polyP and reduce oxidative stress-associated DNA damage. Nudt3 is broadly expressed in human tissues but particularly in the brain, a tissue with high levels of sequestered Zn^{2+}. Thus, we conclude that Nudt3 represents a physiological endo-polyPase that may serve important roles in brain stress tolerance.

Ion requirements, structural considerations, and substrate specificity

That Nudt3 can be activated by multiple cations is an intriguing characteristic shared with other polyPases (Andreeva et al., 2015). Although this fact could represent a way of producing several enzymatic activities using very few genetic resources, how the cation can confer the substrate specificity remains unknown. The crystal structure of Nudt3 suggests three Mg^{2+} binding sites (Thorsell et al., 2009) that might be alternatively bound by Mg^{2+}, Mn^{2+}, or Zn^{2+} to alter substrate specificity forcing a specific orientation for each substrate. The binding of Zn^{2+} to polyP (Sanz-Luque et al., 2020) might bend the polyP molecule in a conformation that could make it more susceptible to be hydrolyzed by Nudt3.

Mg^{2+} is the most abundant divalent cation in the cells, with a concentration that remains close to 1 mM under many physiological cellular responses (de Baaij et al., 2015). By contrast, most other cations are kept sequestered via high-affinity binding and/or sequestration in membranous organelles. Although Zn^{2+} is an essential cofactor for many proteins, free Zn^{2+} is held in the low nanomolar range (Krezel and Maret, 2006), in part via buffering by MTs. However, bound Zn^{2+} can be released upon oxidation of MT cysteine thiols (Krezel and Maret, 2007; Li and Maret, 2008; Maret and Vallee, 1998) during oxidative stress, leading to an increase in cellular Zn^{2+} activity. Of note, a role for Zn^{2+} as an intracellular messenger in the brain is well known (Yamasaki et al., 2007), and some MTs, such as MT3, are specifically expressed in the brain (Genotype-Tissue Expression [GTEx] Portal), suggesting a relevant role for Zn^{2+} in this particular organ (Pearce et al., 2000; Spahl et al., 2003). Importantly, it should be considered that, in rats, the amount of brain polyP reduces progressively with aging (Lorenz et al., 1997), as it does in Alzheimer's mouse models (Cremers et al., 2016). It is also of great significance to note that polyP reduction correlates with a higher Zn^{2+} content in neurodegenerative diseases (Frederickson et al., 2005). All together, these results underline the importance of Zn^{2+}, Nudt3, and polyP in brain physiology.

Almost half of the cellular Zn^{2+} is nuclear (Vallee and Falchuk, 1993) where polyP is predominant, as shown in our results and by others (Jimenez-Nuñez et al., 2012; Negreiros et al., 2018; Xie et al., 2019). Nudt3 has been considered to be cytoplasmic (McLennan, 2006) mainly because of its decapping activity (Sheth and Parker, 2003). However, we present here immunolocalization evidence showing Nudt3's ubiquitous localization. Considering all this, it is very plausible that polyP, Zn^{2+}, and Nudt3 could be in the same compartment, giving spatial coherence to the Nudt3/Zn^{2+}-dependent polyPase activity.

Along with substrate switching by cations, competition between Nudt3 substrates has been demonstrated, raising the question of whether the reduction in polyP content is a direct

Figure 4. Nudt3 is a Zn^{2+}-dependent polyPase *in vivo*

(A) Zn^{2+} decreases nuclear polyP content. HEK293T cells were grown with 100 μM Zn^{2+} in the medium and with the chelators EDTA or NaHS (200 μM) for 48 h. Polyphosphate was detected as in Figure 3A. Representative pictures are in the left panel. Quantification of at least 10 pictures from three independent experiments is in the right panel. A minimum of 500 cells per condition were analyzed. Mean ± SEM is provided.

(B) Mg^{2+} does not affect nuclear polyP content. HEK293T cells were grown in the presence of Zn^{2+} or Mg^{2+} (100 μM) for 24 and 48 h. Polyphosphate was detected, and representative pictures are in the left panel. Quantification of five pictures containing more than 200 cells per condition from one experiment is presented.

(C) Zn^{2+} controls polyP content in the brain cell line SH-SY5Y. Cells were grown in the presence of 100 μM Zn^{2+} for 24 and 48 h. Polyphosphate was detected, and representative pictures are in the left panel. Quantification of three pictures containing a minimum of 100 cells from one experiment.

(D) Zn^{2+} effect on polyP is dependent on Nudt3. Nudt3 was silenced in HEK293T cells and after 24 h, 100 μM Zn^{2+} was added. Polyphosphate was detected after 24 h. Representative pictures are in the left panel. Quantification of 15 pictures from three independent experiments is in the right panel. A minimum of 300 cells per condition were analyzed. Mean ± SEM is provided.

(E) Inositol pyrophosphate ($InsP_7$) is not affected by Zn^{2+}. HEK293T cells were grown in the presence of 100 μM Zn^{2+} or Mg^{2+} for 24 and 48 h. Cells were treated with 10 mM NaF for 1 h to raise the $InsP_7$ intracellular levels and ensure its visualization in a 35% PAGE gel. $InsP_6$ was included as a size marker at the left line. The scale bars represent 10 μm. NT, not treated. See also Figure S2. ***$p < 0.001$; **$p < 0.01$; *$p < 0.05$.

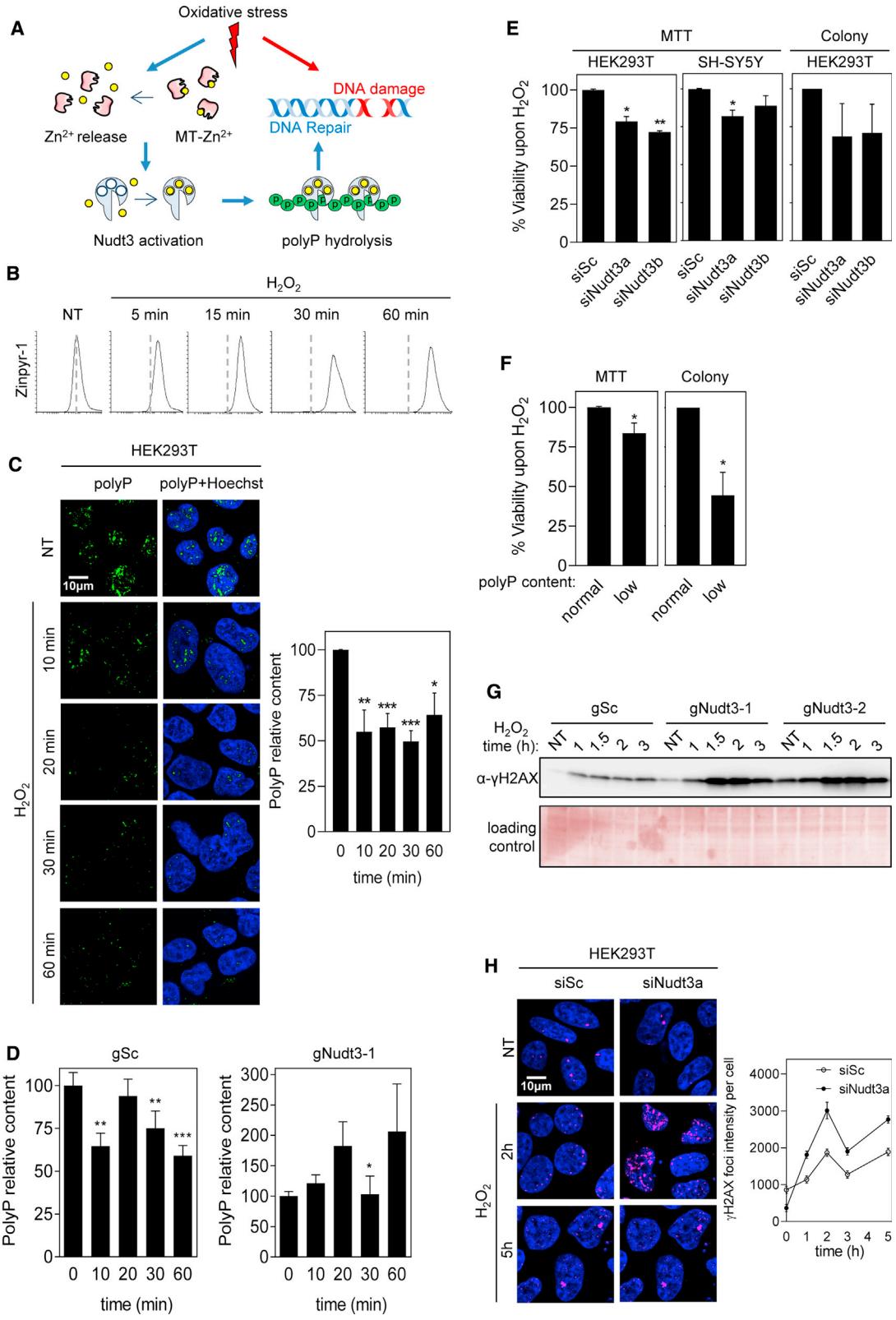

(legend on next page)

effect of its polyP activity or a consequence of its previously reported IP_7/IP_8 hydrolase activity (Kilari et al., 2013; Safrany and Shears, 1998). Our polyP-zymogram analysis of the peak of *in vivo* activity and multiple *in vitro* enzyme assays on purified and recombinant Nudt3 each confirms Zn^{2+}-inducible endo-polyPase activity by Nudt3. Further, Zn^{2+} does not affect InsP7 levels under conditions where polyP becomes destabilized. Note that InsP7 is already comparatively low in HEK293T (Qiu et al., 2020), further arguing against a competitive inhibition or indirect action model. In summary, we propose that Nudt3 is a Zn^{2+}-dependent endo-polyPase that directly regulates polyP levels in mammalian cells.

PolyP and its role in oxidative stress protection, a working model

Among many other functions, polyP has been elegantly proposed to serve a chaperone-like function in bacteria to limit aggregation of damaged proteins during oxidative stress (Gray et al., 2014). Although chaperone function in polyP pools recalcitrant to Nudt3 degradation could be conserved in mammalian cells, our results point to polyP hydrolysis in response to oxidative stress in metazoan cells via Zn^{2+} release and activation of Nudt3 polyPase activity. Different mechanistic possibilities could explain the role of polyP degradation in oxidative stress response. First, polyP hydrolysis might represent the source of ATP needed for cell repair mechanisms as established for Nudt5 (Wright et al., 2016) and in several microbial models where polyP is necessary for ADP-to-ATP turnover (Borden et al., 2021; McIntyre and Solesio, 2021). However, our results show that ATP levels do not change under conditions where polyP is degraded. Second, phospho-transfer from polyP might be critical for dNTP synthesis and DNA repair (Bru et al., 2017). Taking into account that foci of highly concentrated dNTPs are essential for DNA repair in mammalian cells (Niida et al., 2010), the possibility emerges that nuclear polyP degradation could be needed for dealing with the DNA damage produced by oxidative stress. Third, polyP is a poly-anion able to bind proteins electrostatically (Cremers et al., 2016; Gray et al., 2014) and thereby may serve a role in sequestering specific nuclear proteins (Negreiros et al., 2018). PolyP complexed with cationic proteins can form a condensate and display liquid droplet phase separation both *in vitro* and in bacterial cells (Wang et al., 2020). The nuclear polyP foci observed here in human cells might represent analogous polyP-protein condensates, perhaps serving not only as a source of high-energy phosphates but also as a reservoir of proteins available to accelerate repair. Thereby, Zn^{2+} release, activation of Nudt3, and polyP cleavage and depolymerization might release these proteins to participate in stress response.

Limitations of this work

The polyP measurements and *in vivo* experiments were performed in cell lines growing in flat cultures. PolyP quantification in both PAGE gels and immuno-localization was performed by image analysis.

STAR★METHODS

Detailed methods are provided in the online version of this paper and include the following:

- KEY RESOURCES TABLE
- RESOURCE AVAILABILITY
  - Lead contact
  - Materials availability
  - Data and code availability
- EXPERIMENTAL MODEL AND SUBJECT DETAILS
- METHOD DETAILS
  - Cell lines transfection
  - Plasmids and recombinant proteins

Figure 5. Nudt3 Zn^{2+}-dependent polyP degradation is needed for cell viability upon oxidative stress

(A) Working model. Oxidative stress leads to DNA damage and acts on the redox-sensitive metallothioneins (MTs) determining the release of intracellular Zn^{2+}, which, in turn, activates the polyPase activity of Nudt3 and the depletion of polyP. The degradation of polyP protects DNA from oxidative damage and, as a result, cell viability is increased.

(B) Oxidative stress increases intracellular free Zn^{2+} in HEK293T. Cells were exposed to 50 μM H_2O_2 at the indicated times, treated with Zinpyr for 1 h, and the green fluorescence intensity was measured by FACS analysis. 10,000 events were recorded.

(C) Oxidative stress reduces polyP content. HEK293T cells were treated with 30 μM H_2O_2 for the noted time and immediately fixed. Polyphosphate content was detected, and representative pictures are in the left panel. The quantification of three independent experiments is in the right panel. The mean ± SEM is provided. A minimum of 400 cells per condition were analyzed.

(D) PolyP reduction upon oxidative stress is Nudt3 dependent. HEK293T cells, in which Nudt3 has been depleted by CRISPR-Cas, were treated with 30 μM H_2O_2 for the noted times and immediately fixed. Scrambled guide (gSc) is used as control and gNudt3-1 is the specific guide for targeting Nudt3 gen. Polyphosphate content was detected by immunofluorescence as in Figure 3A. The graph represents the quantification of three independent experiments. The mean ± SEM is provided. A minimum of 400 cells per condition were analyzed.

(E and F) Cell viability upon oxidative stress is dependent on Nudt3 polyPase activity. (E) Nudt3 was silenced in HEK293T and SH-SY5Y. After 48 h, 30 μM H_2O_2 was added, and 24 h later, MTT was performed. In the case of colony formation assays, cells were treated with 100 μM H_2O_2 for 1 h. Mean ± SEM from three independent experiments is shown. (F) Nudt3 was overexpressed as in Figure 3C (note that overproduction of Nudt3 leads to polyP depletion, noted as low polyP content. This effect is similar to being unable to use polyP as a result of Nudt3 silencing). Viability was measured as MTT and colony-forming in HEK293T cells were grown in the absence or presence of 30 μM H_2O_2 for 24 h (for the MTT experiments) and 100 μM for 1 h for the colony-forming assays. Mean ± SEM from three independent experiments is represented.

(G and H) DNA damage upon oxidative stress is Nudt3 dependent. (G) Nudt3 was knocked down in HEK293T cells by using two different CRISPR-Cas9 guides. After 72 h, cells were treated with 100 μM H_2O_2 for 1 h and washed with fresh medium. Histone H2AX phosphorylation was detected by western blot with specific antibodies. Time is from the moment in which H_2O_2 was added. (H) Nudt3 was silenced in HEK293T cells. After 48 h cells were treated with 100 μM H_2O_2 for 1 h and washed with fresh medium. Histone phosphorylated foci were detected by immunofluorescence (using specific antibodies as in G). Representative images and fluorescence intensity (mean ± SEM) quantification from one experiment where a minimum of 250 cells were analyzed.

The scale bars represent 10 μm. See also Figures S3 and S4. ***$p < 0.001$; **$p < 0.01$; *$p < 0.05$.

- Cell extracts, western blot, and Ponceau staining
- Small interfering RNA (siRNA)
- CRISPR Cas9
- Biological samples and endo-polyPase purification
- polyP-zymogram
- PAGE-urea gels and polyP electrophoresis
- Endo-polyPase activity quantification
- Malachite green exo-polyPase activity assay
- Inositol pyrophosphatase assay
- Dinucleoside polyphosphatase activity
- Viability assays
- Polyphosphate tissue extraction
- Microscopy and polyP immunolocalization
- ATP measurement
- Intracellular Zn^{2+} measurement
- Zebrafish maintenance
- crRNA design
- Ribonucleoprotein complex (Cas9+gRNA) microinjection for F0 knock-out
- Zebrafish Genomic DNA extraction
- Zebrafish amplification of fragments

● QUANTIFICATION AND STATISTICAL ANALYSIS

SUPPLEMENTAL INFORMATION

Supplemental information can be found online at https://doi.org/10.1016/j.celrep.2021.110004.

ACKNOWLEDGMENTS

We thank Cristina Acevedo and Felix Ruiz for the helpful discussion, Sebastián Zagmutt for helping with the graphical abstract, Toshikazu Shiba (RegeneTiss) for $polyP_{100}$, Miguel Beato and Roni Wright (CRG Barcelona) for Nudt5 protein, and the Helleday Laboratory (Karolinska Institute) for the NUDIX plasmids. The data used for the analyses described in this manuscript were obtained from the GTEx Portal, supported by the Common Fund of the Office of the Director of the National Institutes of Health and by NCI, NHGRI, NHLBI, NIDA, NIMH, and NINDS. This work was supported by and is part of the I+D+i grant ref. PGC2018-096597-B-I00 (to J.J.) by the Spanish Ministerio de Ciencia e Innovación (MCIN). B.S.-M. was the recipient of a grant from the Agència de Gestió d'Ajuts Universitaris i de Recerca AGAUR ref. 2016FI_B 00025. H.J.J. was supported by the Deutsche Forschungsgemeinschaft (DFG) under Germany's Excellence Strategy (CIBBS, EXC-2189, Project ID 390939984).

AUTHOR CONTRIBUTIONS

B.S.-M., A.S., M.P.-M., R.R.-R., A.B., D.W., and A.S. were in charge of the investigation. H.J.J. and B.A. provided resources. B.A., S.J.K., and A.S. helped with the conceptualization and reviewed and edited the original draft. J.C., J.J., and S.B. did the conceptualization, supervision, funding acquisition, and wrote the original draft.

DECLARATION OF INTERESTS

The authors declare no competing interests.

Received: June 3, 2021
Revised: October 8, 2021
Accepted: October 22, 2021
Published: November 16, 2021

REFERENCES

Aizenman, E., Stout, A.K., Hartnett, K.A., Dineley, K.E., McLaughlin, B., and Reynolds, I.J. (2000). Induction of neuronal apoptosis by thiol oxidation: putative role of intracellular zinc release. J. Neurochem. *75*, 1878–1888.

Albi, T., and Serrano, A. (2016). Inorganic polyphosphate in the microbial world. Emerging roles for a multifaceted biopolymer. World J. Microbiol. Biotechnol. *32*, 27.

Andreeva, N., Trilisenko, L., Eldarov, M., and Kulakovskaya, T. (2015). Polyphosphatase PPN1 of Saccharomyces cerevisiae: switching of exopolyphosphatase and endopolyphosphatase activities. PLoS ONE *10*, e0119594.

Azevedo, C., Livermore, T., and Saiardi, A. (2015). Protein polyphosphorylation of lysine residues by inorganic polyphosphate. Mol. Cell *58*, 71–82.

Babes, V. (1895). Beobachtungen über die metachromatischen Körperchen, Sporenbildung, Verzweigung, Kolben-undKapsel-bildung pathogener Bakerien. Zitschr. f. Hygiene *20*, 412–437.

Beyersmann, D., and Haase, H. (2001). Functions of zinc in signaling, proliferation and differentiation of mammalian cells. Biometals *14*, 331–341.

Bondy-Chorney, E., Abramchuk, I., Nasser, R., Holinier, C., Denoncourt, A., Baijal, K., McCarthy, L., Khacho, M., Lavallée-Adam, M., and Downey, M. (2020). A Broad Response to Intracellular Long-Chain Polyphosphate in Human Cells. Cell Rep. *33*, 108318.

Borden, E.A., Furey, M., Gattone, N.J., Hambardikar, V.D., Liang, X.H., Scoma, E.R., Abou Samra, A., D-Gary, L.R., Dennis, D.J., Fricker, D., et al. (2021). Is there a link between inorganic polyphosphate (polyP), mitochondria, and neurodegeneration? Pharmacol. Res. *163*, 105211.

Brown, M.R., and Kornberg, A. (2004). Inorganic polyphosphate in the origin and survival of species. Proc. Natl. Acad. Sci. USA *101*, 16085–16087.

Bru, S., Jiménez, J., Canadell, D., Ariño, J., and Clotet, J. (2016). Improvement of biochemical methods of polyP quantification. Microb. Cell *4*, 6–15.

Bru, S., Samper-Martín, B., Quandt, E., Hernández-Ortega, S., Martínez-Laínez, J.M., Garí, E., Rafel, M., Torres-Torronteras, J., Martí, R., Ribeiro, M.P.C., et al. (2017). Polyphosphate is a key factor for cell survival after DNA damage in eukaryotic cells. DNA Repair (Amst.) *57*, 171–178.

Caffrey, J.J., Safrany, S.T., Yang, X., and Shears, S.B. (2000). Discovery of molecular and catalytic diversity among human diphosphoinositol-polyphosphate phosphohydrolases. An expanding Nudt family. J. Biol. Chem. *275*, 12730–12736.

Carreras-Puigvert, J., Zitnik, M., Jemth, A.S., Carter, M., Unterlass, J.E., Hallström, B., Loseva, O., Karem, Z., Calderón-Montaño, J.M., Lindskog, C., et al. (2017). A comprehensive structural, biochemical and biological profiling of the human NUDIX hydrolase family. Nat. Commun. *8*, 1541.

Cordeiro, C.D., Ahmed, M.A., Windle, B., and Docampo, R. (2019). NUDIX hydrolases with inorganic polyphosphate exo- and endopolyphosphatase activities in the glycosome, cytosol and nucleus of *Trypanosoma brucei*. Biosci. Rep. *39*, BSR20190894.

Cremers, C.M., Knoefler, D., Gates, S., Martin, N., Dahl, J.U., Lempart, J., Xie, L., Chapman, M.R., Galvan, V., Southworth, D.R., and Jakob, U. (2016). Polyphosphate: A Conserved Modifier of Amyloidogenic Processes. Mol. Cell *63*, 768–780.

de Baaij, J.H., Hoenderop, J.G., and Bindels, R.J. (2015). Magnesium in man: implications for health and disease. Physiol. Rev. *95*, 1–46.

Desfougères, Y., Saiardi, A., and Azevedo, C. (2020). Inorganic polyphosphate in mammals: where's Wally? Biochem. Soc. Trans. *48*, 95–101.

Frederickson, C.J., Koh, J.Y., and Bush, A.I. (2005). The neurobiology of zinc in health and disease. Nat. Rev. Neurosci. *6*, 449–462.

Gasa, L., Sanchez-Botet, A., Quandt, E., Hernández-Ortega, S., Jiménez, J., Carrasco-García, M.A., Simonetti, S., Kron, S.J., Ribeiro, M.P., Nadal, E., et al. (2017). A systematic analysis of orphan cyclins reveals CNTD2 as a new oncogenic driver in lung cancer. Sci. Rep. *7*, 10228.

Gerasimaitė, R., and Mayer, A. (2017). Ppn2, a novel Zn^{2+}-dependent polyphosphatase in the acidocalcisome-like yeast vacuole. J. Cell Sci. *130*, 1625–1636.

Gray, M.J., Wholey, W.Y., Wagner, N.O., Cremers, C.M., Mueller-Schickert, A., Hock, N.T., Krieger, A.G., Smith, E.M., Bender, R.A., Bardwell, J.C., and Jakob, U. (2014). Polyphosphate is a primordial chaperone. Mol. Cell *53*, 689–699.

Grudzien-Nogalska, E., Jiao, X., Song, M.G., Hart, R.P., and Kiledjian, M. (2016). Nudt3 is an mRNA decapping enzyme that modulates cell migration. RNA *22*, 773–781.

Harold, F.M. (1966). Inorganic polyphosphates in biology: structure, metabolism, and function. Bacteriol. Rev. *30*, 772–794.

Hassanian, S.M., Avan, A., and Ardeshirylajimi, A. (2017). Inorganic polyphosphate: a key modulator of inflammation. J. Thromb. Haemost. *15*, 213–218.

Hoshijima, K., Jurynec, M.J., Klatt Shaw, D., Jacobi, A.M., Behlke, M.A., and Grunwald, D.J. (2019). Highly Efficient CRISPR-Cas9-Based Methods for Generating Deletion Mutations and F0 Embryos that Lack Gene Function in Zebrafish. Dev. Cell *51*, 645–657.e4.

Jiménez, J., Bru, S., Ribeiro, M.P., and Clotet, J. (2017). Polyphosphate: popping up from oblivion. Curr. Genet. *63*, 15–18.

Jimenez-Nuñez, M.D., Moreno-Sanchez, D., Hernandez-Ruiz, L., Benítez-Rondán, A., Ramos-Amaya, A., Rodríguez-Bayona, B., Medina, F., Brieva, J.A., and Ruiz, F.A. (2012). Myeloma cells contain high levels of inorganic polyphosphate which is associated with nucleolar transcription. Haematologica *97*, 1264–1271.

Kilari, R.S., Weaver, J.D., Shears, S.B., and Safrany, S.T. (2013). Understanding inositol pyrophosphate metabolism and function: kinetic characterization of the DIPPs. FEBS Lett. *587*, 3464–3470.

Kornberg, A. (1999). Inorganic polyphosphate: a molecule of many functions. Prog. Mol. Subcell. Biol. *23*, 1–18.

Krezel, A., and Maret, W. (2006). Zinc-buffering capacity of a eukaryotic cell at physiological pZn. J. Biol. Inorg. Chem. *11*, 1049–1062.

Krezel, A., and Maret, W. (2007). Different redox states of metallothionein/thionein in biological tissue. Biochem. J. *402*, 551–558.

Kulaev, I.S., and Vagabov, V.M. (1983). Polyphosphate metabolism in microorganisms. Adv. Microb. Physiol. *24*, 83–171.

Kumble, K.D., and Kornberg, A. (1995). Inorganic polyphosphate in mammalian cells and tissues. J. Biol. Chem. *270*, 5818–5822.

Kumble, K.D., and Kornberg, A. (1996). Endopolyphosphatases for long chain inorganic polyphosphate in yeast and mammals. J. Biol. Chem. *271*, 27146–27151.

Lee, S.R. (2018). Cellular toxicity of zinc can be attenuated by sodium hydrogen sulfide in neuronal SH-SY5Y cell. Mol. Cell. Toxicol. *14*, 425–436.

Li, Y., and Maret, W. (2008). Human metallothionein metallomics. J. Anal. At. Spectrom. *23*, 1055–1062.

Lichko, L., Kulakovskaya, T., and Kulaev, I. (1998). Membrane-bound and soluble polyphosphatases of mitochondria of Saccharomyces cerevisiae: identification and comparative characterization. Biochim. Biophys. Acta *1372*, 153–162.

Lonetti, A., Szijgyarto, Z., Bosch, D., Loss, O., Azevedo, C., and Saiardi, A. (2011). Identification of an evolutionarily conserved family of inorganic polyphosphate endopolyphosphatases. J. Biol. Chem. *286*, 31966–31974.

Lorenz, B., Münkner, J., Oliveira, M.P., Kuusksalu, A., Leitão, J.M., Müller, W.E., and Schröder, H.C. (1997). Changes in metabolism of inorganic polyphosphate in rat tissues and human cells during development and apoptosis. Biochim. Biophys. Acta *1335*, 51–60.

Maret, W. (2000). The function of zinc metallothionein: a link between cellular zinc and redox state. J. Nutr. *130* (*5S Suppl*), 1455S–1458S.

Maret, W. (2011). Redox biochemistry of mammalian metallothioneins. J. Biol. Inorg. Chem. *16*, 1079–1086.

Maret, W., and Vallee, B.L. (1998). Thiolate ligands in metallothionein confer redox activity on zinc clusters. Proc. Natl. Acad. Sci. USA *95*, 3478–3482.

McIntyre, B., and Solesio, M.E. (2021). Mitochondrial inorganic polyphosphate (polyP): the missing link of mammalian bioenergetics. Neural Regen. Res. *16*, 2227–2228.

McLennan, A.G. (2006). The Nudix hydrolase superfamily. Cell. Mol. Life Sci. *63*, 123–143.

Morimoto, D., Tomita, T., Kuroda, S., Higuchi, C., Kato, S., Shiba, T., Nakagami, H., Morishita, R., and Yoshikawa, H. (2010). Inorganic polyphosphate differentiates human mesenchymal stem cells into osteoblastic cells. J. Bone Miner. Metab. *28*, 418–423.

Negreiros, R.S., Lander, N., Huang, G., Cordeiro, C.D., Smith, S.A., Morrissey, J.H., and Docampo, R. (2018). Inorganic polyphosphate interacts with nucleolar and glycosomal proteins in trypanosomatids. Mol. Microbiol. *110*, 973–994.

Nickel, K.F., Ronquist, G., Langer, F., Labberton, L., Fuchs, T.A., Bokemeyer, C., Sauter, G., Graefen, M., Mackman, N., Stavrou, E.X., et al. (2015). The polyphosphate-factor XII pathway drives coagulation in prostate cancer-associated thrombosis. Blood *126*, 1379–1389.

Niida, H., Katsuno, Y., Sengoku, M., Shimada, M., Yukawa, M., Ikura, M., Ikura, T., Kohno, K., Shima, H., Suzuki, H., et al. (2010). Essential role of Tip60-dependent recruitment of ribonucleotide reductase at DNA damage sites in DNA repair during G1 phase. Genes Dev. *24*, 333–338.

Pavlov, E., Aschar-Sobbi, R., Campanella, M., Turner, R.J., Gómez-García, M.R., and Abramov, A.Y. (2010). Inorganic polyphosphate and energy metabolism in mammalian cells. J. Biol. Chem. *285*, 9420–9428.

Pearce, L.L., Gandley, R.E., Han, W., Wasserloos, K., Stitt, M., Kanai, A.J., McLaughlin, M.K., Pitt, B.R., and Levitan, E.S. (2000). Role of metallothionein in nitric oxide signaling as revealed by a green fluorescent fusion protein. Proc. Natl. Acad. Sci. USA *97*, 477–482.

Qiu, D., Wilson, M.S., Eisenbeis, V.B., Harmel, R.K., Riemer, E., Haas, T.M., Wittwer, C., Jork, N., Gu, C., Shears, S.B., et al. (2020). Analysis of inositol phosphate metabolism by capillary electrophoresis electrospray ionization mass spectrometry. Nat. Commun. *11*, 6035.

Ran, F.A., Hsu, P.D., Wright, J., Agarwala, V., Scott, D.A., and Zhang, F. (2013). Genome engineering using the CRISPR-Cas9 system. Nat. Protoc. *8*, 2281–2308.

Riley, A.M., Unterlass, J., Konieczny, V., Taylor, C.W., Helleday, T., and Potter, B.V.L. (2018). A synthetic diphosphoinositol phosphate analogue of inositol trisphosphate. MedChemComm *9*, 1105–1113.

Safrany, S.T., and Shears, S.B. (1998). Turnover of bis-diphosphoinositol tetrakisphosphate in a smooth muscle cell line is regulated by beta2-adrenergic receptors through a cAMP-mediated, A-kinase-independent mechanism. EMBO J. *17*, 1710–1716.

Safrany, S.T., Caffrey, J.J., Yang, X., Bembenek, M.E., Moyer, M.B., Burkhart, W.A., and Shears, S.B. (1998). A novel context for the 'MutT' module, a guardian of cell integrity, in a diphosphoinositol polyphosphate phosphohydrolase. EMBO J. *17*, 6599–6607.

Safrany, S.T., Caffrey, J.J., Yang, X., and Shears, S.B. (1999). Diphosphoinositol polyphosphates: the final frontier for inositide research? Biol. Chem. *380*, 945–951.

Sahu, S., Wang, Z., Jiao, X., Gu, C., Jork, N., Wittwer, C., Li, X., Hostachy, S., Fiedler, D., Wang, H., et al. (2020). $InsP_7$ is a small-molecule regulator of NUDT3-mediated mRNA decapping and processing-body dynamics. Proc. Natl. Acad. Sci. USA *117*, 19245–19253.

Saito, K., Ohtomo, R., Kuga-Uetake, Y., Aono, T., and Saito, M. (2005). Direct labeling of polyphosphate at the ultrastructural level in Saccharomyces cerevisiae by using the affinity of the polyphosphate binding domain of Escherichia coli exopolyphosphatase. Appl. Environ. Microbiol. *71*, 5692–5701.

Sanz-Luque, E., Bhaya, D., and Grossman, A.R. (2020). Polyphosphate: A Multifunctional Metabolite in Cyanobacteria and Algae. Front. Plant Sci. *11*, 938.

Sheth, U., and Parker, R. (2003). Decapping and decay of messenger RNA occur in cytoplasmic processing bodies. Science *300*, 805–808.

Smith, S.A., Mutch, N.J., Baskar, D., Rohloff, P., Docampo, R., and Morrissey, J.H. (2006). Polyphosphate modulates blood coagulation and fibrinolysis. Proc. Natl. Acad. Sci. USA *103*, 903–908.

Spahl, D.U., Berendji-Grün, D., Suschek, C.V., Kolb-Bachofen, V., and Kröncke, K.D. (2003). Regulation of zinc homeostasis by inducible NO synthase-derived NO: nuclear metallothionein translocation and intranuclear Zn2+ release. Proc. Natl. Acad. Sci. USA *100*, 13952–13957.

Stankovic, R.K., Chung, R.S., and Penkowa, M. (2007). Metallothioneins I and II: neuroprotective significance during CNS pathology. Int. J. Biochem. Cell Biol. *39*, 484–489.

Stepanenko, A.A., and Dmitrenko, V.V. (2015). HEK293 in cell biology and cancer research: phenotype, karyotype, tumorigenicity, and stress-induced genome-phenotype evolution. Gene *569*, 182–190.

Tammenkoski, M., Koivula, K., Cusanelli, E., Zollo, M., Steegborn, C., Baykov, A.A., and Lahti, R. (2008). Human metastasis regulator protein H-prune is a short-chain exopolyphosphatase. Biochemistry *47*, 9707–9713.

Thorsell, A.G., Persson, C., Gräslund, S., Hammarström, M., Busam, R.D., and Hallberg, B.M. (2009). Crystal structure of human diphosphoinositol phosphatase 1. Proteins *77*, 242–246.

Travers, R.J., Smith, S.A., and Morrissey, J.H. (2015). Polyphosphate, platelets, and coagulation. Int. J. Lab. Hematol. *37* (*Suppl 1*), 31–35.

Vallee, B.L., and Falchuk, K.H. (1993). The biochemical basis of zinc physiology. Physiol. Rev. *73*, 79–118.

Wang, L., Fraley, C.D., Faridi, J., Kornberg, A., and Roth, R.A. (2003). Inorganic polyphosphate stimulates mammalian TOR, a kinase involved in the proliferation of mammary cancer cells. Proc. Natl. Acad. Sci. USA *100*, 11249–11254.

Wang, X., Shi, C., Mo, J., Xu, Y., Wei, W., and Zhao, J. (2020). An Inorganic Biopolymer Polyphosphate Controls Positively Charged Protein Phase Transitions. Angew. Chem. Int. Ed. Engl. *59*, 2679–2683.

Werner, T.P., Amrhein, N., and Freimoser, F.M. (2005). Novel method for the quantification of inorganic polyphosphate (iPoP) in Saccharomyces cerevisiae shows dependence of iPoP content on the growth phase. Arch. Microbiol. *184*, 129–136.

Westerfield, M., Doerry, E., and Douglas, S. (1999). Zebrafish in the Net. Trends Genet. *15*, 248–249.

Wright, R.H., Lioutas, A., Le Dily, F., Soronellas, D., Pohl, A., Bonet, J., Nacht, A.S., Samino, S., Font-Mateu, J., Vicent, G.P., et al. (2016). ADP-ribose-derived nuclear ATP synthesis by NUDIX5 is required for chromatin remodeling. Science *352*, 1221–1225.

Wu, R.S., Lam, I.I., Clay, H., Duong, D.N., Deo, R.C., and Coughlin, S.R. (2018). A Rapid Method for Directed Gene Knockout for Screening in G0 Zebrafish. Dev. Cell *46*, 112–125.e4.

Xie, L., Rajpurkar, A., Quarles, E., Taube, N., Rai, A.S., Erba, J., Sliwinski, B., Markowitz, M., Jakob, U., and Knoefler, D. (2019). Accumulation of Nucleolar Inorganic Polyphosphate Is a Cellular Response to Cisplatin-Induced Apoptosis. Front. Oncol. *9*, 1410.

Yamasaki, S., Sakata-Sogawa, K., Hasegawa, A., Suzuki, T., Kabu, K., Sato, E., Kurosaki, T., Yamashita, S., Tokunaga, M., Nishida, K., and Hirano, T. (2007). Zinc is a novel intracellular second messenger. J. Cell Biol. *177*, 637–645.

STAR★METHODS

KEY RESOURCES TABLE

REAGENT or RESOURCE	SOURCE	IDENTIFIER
Antibodies		
Rabbit Anti-Nudt3	Sigma Aldrich	Ref: SAB2700523; RRID: AB_2894928
Mouse monoclonal anti-Xpress	Life and Technologies	Ref: 46-0528; RRID: AB_2556552
Mouse Anti-Flag	Sigma Aldrich	Ref: F3165; RRID: AB_259529
Rabbit Anti-GFP	Cell Signaling	Ref: 29565; RRID: AB_1196615
Mouse γH2AX	Millipore	Ref: 05-636; RRID: AB_309864
Alexa Fluor 488 conjugated goat anti mouse	Invitrogen	Ref: A11001; RRID: AB_2534069
AlexaFluor 633 conjugated goat anti mouse	Invitrogen	Ref: A21052; RRID: AB_2535719
HRP-Goat Anti-Rabbit IgG	Jackson Immuno Research	Ref: 111-035-144; RRID: AB_2307391
Bacterial and virus strains		
E. coli DL21 DE3	Bio-RAD	Ref: 1563003
Biological samples		
Rattus norvegicus brain (Sprague Dawley)	UB animal facility	N/A
Chemicals, peptides, and recombinant proteins		
C-Myc/DDK-Nudt3	Origene	Ref: TP302900
$polyP_{100}$	RegeneTiss	EUI005
$5\text{-}InsP_7$	This work	N/A
Ap_5A	This work	N/A
Critical commercial assays		
ATP determination kit	Molecular Probes	Ref: A22066
ZinPyr	Sigma Aldrich	Ref: AB145349
Experimental models: Cell lines		
HEK293T	ATCC authenticated	N/A
SH-SY5Y	Sigma Aldrich	Ref: 94030304-1vl
Experimental models: Organisms/strains		
Danio rerio	CRG animal facility	N/A
Oligonucleotides		
Nudt3guide1 AGCAGTTCGTGAAGTCTGTG	IDT	N/A
Nudt3guide2 GTAGTCGCCATCCAGACAGA	IDT	N/A
Nudt3A siRNA rGrCrArCrArGrGrArCrGrUrArUrGrUrCrUrArUrGrUGC	IDT	N/A
Nudt3B siRNA rUrArArArArGrUrGrCrUrGrCrArGrUrArUrCrArCrAAA	IDT	N/A
Recombinant DNA		
pGEX6p1-Nudt3	This work. BamHI	N/A
pGEX6p1-Nudt3E70A	This work. BamHI	N/A
pGEX6p1-Nudt4	This work. BamHI	N/A
pGEX6p1-Nudt10	This work. BamHI	N/A
pGEX6p1-Nudt11	This work. BamHI	N/A
pGEX6p1-zNudt3a	This work. BamHI	N/A
pGEX6p1-zNudt3b	This work. BamHI	N/A
pWPI-Nudt3-flag	This work. *Pme*HI	N/A
pWPI-NLS-*PPX1*-flag	This work. *Pme*HI	N/A
pRetroX-Tet-on-Advanced	Takara	Ref: 632104

(*Continued on next page*)

Continued

REAGENT or RESOURCE	SOURCE	IDENTIFIER
pRetroX-Tight-Pur	Takara	Ref: 632104
pRetroX-Tight-Pur-NUDT3	This Work	N/A
pX459	Addgene	Ref: 62988
Software and algorithms		
Image Studio Lite	Li-Cor	N/A
ImageJ	https://imagej.nih.gov/ij/	N/A
Other		
crRNA tool designer Chop-Chop	https://chopchop.cbu.uib.no/	N/A

RESOURCE AVAILABILITY

Lead contact

Further information and request for resources and reagents should be directed to and will be fulfilled by the lead contact, Javier Jiménez (jjimenez@uic.es).

Materials availability

All materials and reagents generated in this work are available from the lead contact upon request.

Data and code availability

- All data reported in this paper will be shared by the lead contact upon request.
- This paper does not report original code.
- Any additional information required to reanalyze the data is available from the lead contact upon request.

EXPERIMENTAL MODEL AND SUBJECT DETAILS

HEK293T (authenticated by ATCC cell authentication service by STR profile report. FTA barcode: STRA6311) and SH-SY5Y (purchased to Sigma Aldrich ref: 94030304-1vl. Lot number 14A035. Test number 51117) cell lines were cultured in Dulbecco's Modified Eagle Medium (Sigma-Aldrich) supplemented with 10% fetal bovine serum (Sigma-Aldrich), 1% glutamax (Biowest, Nuaillé) and 1% penicillin/streptomycin (Sigma-Aldrich). All cells were grown in humidified air at 37°C and 5% CO_2 atmosphere. Mycoplasma contamination was monitored periodically.

METHOD DETAILS

Cell lines transfection

$CaCl_2$ method was used to transfect plasmids as follows: cell medium was changed 2 h before transfection. 0.75 μg of plasmid to be transfected was included in the following mix (final concentration): Tris -EDTA (3 mM and 0.3 mM respectively); 2.5 mM HEPES pH 7.3; 18.5 mM $CaCl_2$; HeBS (280 mM NaCl, 50 mM HEPES, 1.5 mM $Na_2HPO\text{-}2H_2O$). The solution was carefully added to the well, gently agitated to obtain homogeneous color, and incubated overnight at 37°C in a 5% CO_2 containing atmosphere.

Lipofectamine 2000 system was used to transfect siRNAs. The protocol was as indicated by the purchaser. In short, for each transfection, 100 μL of the transfecting mix was added to every well. Transfecting mix includes 12.5 pmol siRNA oligomer (25 nM final concentration) in 50 μL of culture medium without serum or penicillin-streptomycin and 50 μL of lipofectamine mix (0.5 μL of lipofectamine 2000 in 50 μL of culture medium without serum or antibiotics). Both components, previously kept at room temperature for 5 min, were mixed gently and incubated for 20 min at room temperature. Once the lipofectamine-siRNA was added to the cells, the plates were gently agitated and incubated at 37°C in a 5% CO_2 containing atmosphere for 24-48 h.

Plasmids and recombinant proteins

Plasmids are in the key resources table. HEK293T human cell line cDNA was used to amplify the different NUDIX genes. All of them were cloned into a pGEX6P1 vector (Cytiva ref: 28954648). Site-directed mutagenesis of Nudt3 was performed by PCR using oligonucleotides containing the desired change. Nudt5 was a present from Dr. M. Beato (CRG Barcelona). For expression of the recombinant proteins, pGEX6P1 NUDIX containing plasmids were transformed into BL21 DE3 cells (Bio-RAD). Purification was performed as indicated by the purchaser.

Cell extracts, western blot, and Ponceau staining

Cell extracts and western blot were as described in (Gasa et al., 2017). For antibodies, see the key resources table. Detection was done with Luminata Forte Western HRP Substrate (Millipore) and images were taken using the GeneSnap (Syngene) software. The density of the bands was analyzed using the Image Studio Lite (Li-Cor) software and Ponceau staining (Sigma-Aldrich) was used to normalize sample load.

Small interfering RNA (siRNA)

HEK293T and SH 5YSY cells were seeded in 24-well plates at a density of 25,000 cells per well. Cells were transfected the following day with Nudt3A siRNA, Nudt3B siRNA (See key resources table), or scrambled (51-01-14-04, IDT) using Lipofectamine 2000 (12566014, Thermo Fisher Scientific).

CRISPR Cas9

The pSpCas9(BB)-2A-Puro (pX459) V2.0 vector was obtained from Addgene (Cambridge, MA, USA; plasmid #62988). The Nudt3-specific RNA guides (see Nudt3guide1 and Nudt3guide2 in the key resources table) were selected using the design tool BENCHLING and purchased from IDT. The gRNA was cloned into pX459 as described elsewhere (Ran et al., 2013). HEK293T cells were transfected with 1 μg of gRNA plasmid DNA (final concentration, 10 μM) using FuGENE HD (Promega).

Biological samples and endo-polyPase purification

The protocols for animal care and use were approved by the Clinical Research Ethics Committee of the University of Barcelona (Procedure Ref. 11113, Generalitat de Catalunya). All experimental animal procedures were carried out in strict accordance with European directive 2010/63/EU and Spanish legislation (BOE 252/34367-91, 2005) regulating animal research. All efforts were made to minimize animal suffering and the number of animals used. Animals were housed according to a 12h/12h light/dark cycle (from 8am to 8pm) in a temperature- and humidity-controlled room, and were allowed free access to water and standard laboratory chow diet. Animals were sacrificed by cervical dislocation under anesthesia and brain was quickly removed and processed.

Protein purification has been performed by the ICTS "NANBIOSIS," more specifically by the Protein Production Platform of CIBER in Bioengineering, Biomaterials & Nanomedicine (CIBER-BBN)/ IBB, at the UAB SePBioEs scientific-technical service. A Sprague Dawley male rat (weight 300 g) brain was obtained and homogenized. Proteins were extracted with 30 ml/gr of lysis buffer (20 mM Tris-HCl pH 8; 1 mM β-mercaptoethanol; 1 mM EDTA; 2% glycerol and protease inhibitors (1 ug/ml pepstatin; 1 ug/ml leupeptin; 1 mM benzamidine and 1 mM PMSF)) and were lysed with 1.4 mm ceramic beads (QIAGEN) in the FastPrep (FastPrep-24 from MP Biomedicals). All following steps were performed in the gel. The glass beads were removed by centrifugation at 2,000 rpm for 2 min. The supernatant was sonicated three times, 30 s with 1 min interval for cooling. The sonicate was centrifuged twice for 15 min at 12,000 rpm and the supernatant was applied to a ÄktaStart protein purification system 5 mL HiTrap Heparin HP affinity column (GE Healthcare Life Science) previously equilibrated with lysis buffer. The column was washed with a 1-bed volume of lysis buffer and eluted with sequentially bed volumes of a NaCl gradient (from 0-1.2 M). Fractions were concentrated with an Amicon Ultra-15 Centrifugal Filters of 10,000 MWCO (Merck) to a final volume of 0.5 ml. The fraction showing endo-polyPase activity (0.5 M NaCl), was added to a Äkta pure Superdex 200 Increase 10/300 GL (GE Healthcare Life Science) previously equilibrated with buffer A (20mM Tris-HCl pH 7.4; 150 mM NaCl; 100 mM NH_4OH; 5 mM $ZnSO_4$). Buffer A was used to collect 24 fractions of 1 ml. The fractions were concentrated with an Amicon Ultra-15 Centrifugal Filters of 10,000 MWCO (Merck) to a final volume of 0.5 ml. The endo-polyPase activity was obtained in fractions 18-19 corresponding to 15.5-23.5 kDa. The endo-polyPase activity for these fractions was assayed in a polyP-zymogram gel and bands were cut and processed for proteomic analysis.

polyP-zymogram

The non-denaturing gels were 10% (37.5:1) acrylamide/bisacrylamide TBE gels (Tris-HCl 0.13 M /Boric acid 45 mM/ EDTA 2.5 mM pH 8.5). The running buffer was TBE containing 4 g/l commercial $polyP_{100}$ (kindly provided by T. Shiba from RegeneTiss). 100-200 ng of the protein sample were included in sample buffer (5X TBE, 7.3 mM sucrose, and bromophenol blue). Before running the sample, 5 μg of commercial $polyP_{100}$ were loaded into the gel and 150 V were applied until the bromophenol blue entered around 2 cm into the gel. After this, the samples were loaded and kept under 150 V for 3 h. After the electrophoresis, the gel was incubated in reaction buffer (20 mM Tris-HCl pH 6.8, 100 mM ammonium acetate, and 5 mM zinc sulfate) for 1 h at 37°C. Polyphosphate was visualized by DAPI staining of the gel; for this, DAPI (7.2 μM) was added to the fixing solution, incubated for 1 h at room temperature. The destaining was done by washing the gel twice for 30 min using the fixing solution but without DAPI. Gels were visualized in a Synergy HT trans-illuminator from Biotek Instruments.

PAGE-urea gels and polyP electrophoresis

Acrylamide gels (15%) containing 7 M urea (17 g urea, 8 mL of 5x TBE (54 g Tris-HCl pH 7.5; 27.5 g of boric acid; 20 mL of 0.5 M EDTA), 27 mL acrylamide/bisacrylamide solution (10:1), 200 μl of ammonium persulfate (10% v/v), 16 μl of TEMED and water to a volume of 50 ml) were cast in a Bio-Rad casting stand (20x20x0.1 cm). Samples containing the polyP to be analyzed were loaded onto the gel by adding 0.2 volumes of loading buffer 6x (TBE, 7.3 mM sucrose, and bromophenol blue). Gels were run for 4 h at 300 V. To visualize polyP, gels were incubated in fixing solution (25% (v/v) methanol and 5% (v/v) glycerol) with DAPI (10 μg/μl)

for 1 h at room temperature. Gels were washed twice for 30 min in fixing solution without DAPI and visualized in a Synergy HT (BioTek Instruments) trans-illuminator.

Endo-polyPase activity quantification

25 μg of rat brain extract or 100 ng of recombinant protein were added to a reaction mix containing 20 mM Tris-HCl pH 6.8, 100 mM ammonium acetate, 5 mM $ZnSO_4$, and 5 μg of $polyP_{100}$ (kindly provided by T. Shiba from RegeneTiss). The temperature was 37°C. The reaction was stopped by adding 0.2 volumes of loading buffer 6x (TBE, 7.3 mM sucrose, and bromophenol blue) and analyzed by PAGE-urea and DAPI staining.

Endo-polyPase activity (nmol/min·mg or ρmol/min·mg) was calculated by measuring the line intensity of the DAPI staining using the software Image Studio Lite (Li-Cor). Intensities were compared to t = 0 to establish the percentage of polyP degradation. Taking into account that the initial amount of polyP and enzyme are known, the amount of degraded polyP, the velocity of the reaction, and the specific activity can be estimated.

Malachite green exo-polyPase activity assay

Exo-polyPase activity assay was as in (Werner et al., 2005). Briefly, the sample to be analyzed was added to a reaction mix containing 20 mM Tris-HCl pH 7.5, 100 mM ammonium acetate, and 5 mM magnesium acetate in a final volume of 100 μl. Released phosphate was quantified by adding 86 μl of 28 mM ammonium heptamolybdate in 2.1 M H_2SO_4 and 64 μl of malachite green solution (0.015% malachite green, 0.1% acetic acid, and 0.17% glycerol). The solution was measured using a microplate spectrophotometer (Synergy HT, Bio Tek Instruments) at 600 nm and compared with phosphate standards (0–500 μM Pi)

Inositol pyrophosphatase assay

Inositol pyrophosphatase activity was measured as in (Riley et al., 2018). Briefly, the sample was incubated in 100 mM Tris-HCl pH 7.5, 40 mM NaCl, 1 mM DTT, 1 mM magnesium acetate, and 5 μg of 5-InsP7 for 90 min at 37°C. Free Pi was quantified by malachite green.

Dinucleoside polyphosphatase activity

Dinucleoside polyphosphatase activity quantification was as in (Riley et al., 2018). Briefly, the sample was incubated in 100 mM Tris-HCl pH 7.5, 40 mM NaCl, 1 mM DTT, 1 mM $MnCl_2$, 5 μg Ap5A (D4022: Sigma-Aldrich) for 90 min at 37°C, and then free Pi was quantified by malachite green.

Viability assays

For colony-forming assays, Nudt3 was silenced or overexpressed in HEK293T cells for 48 h, cells were treated with H_2O_2 for 1 h, trypsinized and 800 cells per well were seeded in a 6 well plate. After 7 days colonies were visible, fixed with 100% cold methanol, washed with PBS, and stained with 0.1% crystal violet for 30 min in the dark.

For MTT analysis, 4 days after transfection (for overexpression or silencing and treatment), cells were incubated with MTT solution (Sigma-Aldrich; M2128) for 1 h at 37°C. The resulting formazan crystals were dissolved in DMSO and the absorbance was measured at 570 nm in a Synergy HT plate reader.

Polyphosphate tissue extraction

Rat brain polyP extraction was as in (Kumble and Kornberg 1995; (Bru et al., 2016)). Briefly, the tissue was suspended in 2.5 volumes of lysis buffer (50 mM Tris-HCl ph7.5, 1 M urea, 0.1% SDS, and 10 mM EDTA) containing 0.25 M sucrose and homogenized using a Polytron for three 10 s pulses and 30 s ice-cooling in between pulses. The lysate was incubated with proteinase K (0.75 mg/ml; 2h at 37°C) and extracted with phenol/chloroform. The polyP was precipitated with barium acetate 0.1 M final concentration pH 4.5 for 4 h at 4°C. After centrifugation and solubilization, the sample was treated with DNase I and RNase A each at 0.35 mg/ml for 1h at 37°C. The sample was deproteinized by extracting with phenol/chloroform and chloroform.

Microscopy and polyP immunolocalization

For polyP immunolocalization, cells were fixed by incubation with 4% paraformaldehyde (v/v) for 15 min at 4°C. For blocking, cells were treated with a PBS solution containing 10% goat serum and 0.5% Tween20 for 1 h at room temperature. Cells were incubated with Xpress-tagged PPBD and anti-Xpress tag antibody (Life Technologies) at a ratio of 20:5 (μg/ml) for 1 h at 4°C in blocking solution. The secondary antibody was (1:1000) Alexa 488 conjugated anti-mouse (Invitrogen) in blocking solution for 1 h in darkness and high humidity conditions. Finally, (1:1000) Hoechst 33342 (Sigma ref: 14530) was added for 5 min at room temperature. Samples were mounted using Fluoromount-G (Southern Biotech, ref: 0100-01). The microscope was a Leica confocal SP8. For polyP quantification, Fiji (ImageJ) software was used. ROIs were selected in the DAPI channel using the filter plugin Gaussian B. To ensure accurate ROIs and to create the mask, threshold, fill holes, and watershed plugins were applied. ROIs mask was overlaid on the polyP channel to obtain the integrated density of every nucleus. The average of polyP integrates density including all microscopy fields was calculated. The graphs represent the difference between the average in the control and the experiment.

ATP measurement

Total cellular ATP content was measured using the ATP determination kit (Molecular Probes). Briefly, Nudt3 was silenced in HEK293T. After 24 h, 30 μM H_2O_2 was added for the indicated times, cells were harvested, permeabilized with 0.1% saponin solution, and the supernatant was used to quantify the total cellular ATP using a microplate reader luminometer as indicated in the kit instructions. The luminometer reads were expressed in arbitrary units.

Intracellular Zn^{2+} measurement

As described in (Lee, 2018). Briefly, ZinPyr (from Sigma) was added to a final concentration of 25 μM for 1 h at 37°C. Cells were fixed adding 4% p-formaldehyde and fluorescence was recorded (excitation 485 nm; emission 595 nm) in a Leica SP8 confocal microscope.

Zebrafish maintenance

Zebrafish (*Danio rerio*) were maintained as previously described (Westerfield et al., 1999) at the aquatic facility of the Parc de Recerca Biomèdica de Barcelona (PRBB). Injections were performed on Ab/Tübingen strain. The sex of zebrafish embryos cannot be assessed.

crRNA design

crRNAs were designed using the online tool Chop-Chop (https://chopchop.cbu.uib.no/) and according to the guidelines from (Wu et al., 2018). As controls, 4 crRNAs that do not target the zebrafish genome were chosen, called *scrambled*. The sequences are in Table S1 named crNudt3a crNudt3b and crScramble.

Ribonucleoprotein complex (Cas9+gRNA) microinjection for F0 knock-out

As described in (Hoshijima et al., 2019). Briefly, target-specific crRNA (36 nucleotides) and common tracrRNA (67 nucleotides) were diluted separately in RNase free TE buffer 1X pH 7.5 to a final concentration of 100 μM. Stocks were stored at −20°C. Equal volumes of crRNA and tracrRNA were added and diluted in IDT Nuclease Free Duplex Buffer to a final concentration of 28 μM (1 μg/μl). The mix was heated at 95°C for 5 min, and then slowly cooled down to room temperature, forming the duplex gRNA (crRNA+tracrRNA). The process was repeated independently for every crRNA. The duplex gRNAs were stored at −20°C. Up to 4 different duplex gRNAs were mixed at equal concentrations in RNase free water, to a final concentration of total duplex gRNAs of 1 μg/μl (250 ng/μl (7.13 μM) of each duplex gRNA if 4 different duplex gRNAs were to be added). PNABio Cas9 (Ref#CP01) protein or S.p. Cas9 Nuclease V3 (Ref# 1081058) protein was added to a final concentration of 300 ng/μl (1.84 μM). The mix (Cas9 + duplex gRNAs + water) was heated at 37°C for 10 min and cooled to room temperature to facilitate the formation of the ribonucleoprotein (RNP) complex. Embryos were injected with 1-2 nL of RNP mix at the 1-cell stage into the cell. Embryos received 1-2 ng of total duplex gRNAs and 300-600 pg Cas9.

Zebrafish Genomic DNA extraction

Genomic DNA was extracted from embryos by alkaline lysis or a commercial kit. For the former, single embryos were placed in 1.5 mL Eppendorf tubes containing 15-50 μl NaOH 5 mM and heated at 95°C 10 min. After that, the tubes were cooled to 4°C. Following, 1/10th of Tris-HCl 1 M pH 8 was added. The mixture was vortexed and centrifuged to pellet debris. From the supernatant, 1-5 μl was taken to do the PCR. 1-5 μl of the PCR was loaded in a 3% agarose gel. Alternatively, we used an XNAT2 Extract-N-Amp Tissue PCR kit. Here, single embryos were placed in 1.5 mL Eppendorf tubes. 10 μl of extraction buffer plus 2.5 μl of tissue preparation was added per tube. Tubes were vortexed and spun down. Tubes were incubated for 10 min at 55°C, then 3 min at 95°C. 10 μl of neutralization buffer was added per tube. After vortexing and spinning, samples were used for PCR, taking 1-5 μl as a template.

Zebrafish amplification of fragments

Genome sequences containing CRISPR/Cas9 target sites were amplified with pairs of primers listed in Table S1 (named CRISPRNudt3a and CRISPRNudt3b). All fragments ranged from 200 to 280 bp. For proper sequencing, Cas9 targeting sites were, at least, 80 bp away from the primer.

QUANTIFICATION AND STATISTICAL ANALYSIS

In endo-polyPase activity experiments, a minimum of three independent experiments were included (particular n values for every experiment can be found in the figure legends), data are represented as the mean ± standard error of the mean (SEM) and statistical significance was determined using the Mann-Whitney test. In Nudt3 activity experiments over the different substrates, ANOVA was used. *p-values*: *** $p < 0.001$; ** $p < 0.01$; * $p < 0.05$. In the microscopy experiments, a minimum of 5 fields with 30-100 cells in each were analyzed. Particular n values for every experiment can be found in the corresponding figure legend. Mann-Whitney was used. Statistical analyses were conducted using GraphPad Prism.